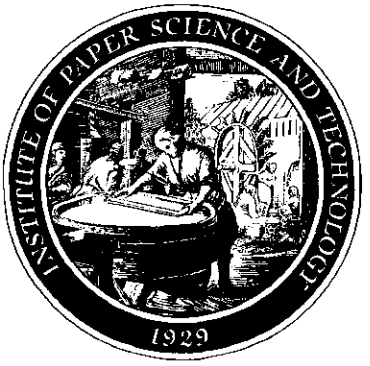

Institute of Paper Science and Technology
Atlanta, Georgia

IPST Technical Paper Series Number 895

Particle Formation of Kraft Smelt in a Fluidized Bed

J. Huff and H.J. Empie

April 2001

Submitted to
Canadian Journal of Chemical Engineering

INSTITUTE OF PAPER SCIENCE AND TECHNOLOGY
PURPOSE AND MISSIONS

The Institute of Paper Science and Technology is an independent graduate school, research organization, and information center for science and technology mainly concerned with manufacture and uses of pulp, paper, paperboard, and other forest products and byproducts. Established in 1929 as the Institute of Paper Chemistry, the Institute provides research and information services to the wood, fiber, and allied industries in a unique partnership between education and business. The Institute is supported by 51 member companies. The purpose of the Institute is fulfilled through four missions, which are:

- to provide a multidisciplinary graduate education to students who advance the science and technology of the industry and who rise into leadership positions within the industry;
- to conduct and foster research that creates knowledge to satisfy the technological needs of the industry;
- to provide the information, expertise, and interactive learning that enables customers to improve job knowledge and business performance;
- to aggressively seek out technological opportunities and facilitate the transfer and implementation of those technologies in collaboration with industry partners.

ACCREDITATION

The Institute of Paper Science and Technology is accredited by the Commission on Colleges of the Southern Association of Colleges and Schools to award the Master of Science and Doctor of Philosophy degrees.

NOTICE AND DISCLAIMER

The Institute of Paper Science and Technology (IPST) has provided a high standard of professional service and has put forth its best efforts within the time and funds available for this project. The information and conclusions are advisory and are intended only for internal use by any company who may receive this report. Each company must decide for itself the best approach to solving any problems it may have and how, or whether, this reported information should be considered in its approach.

IPST does not recommend particular products, procedures, materials, or service. These are included only in the interest of completeness within a laboratory context and budgetary constraint. Actual products, materials, and services used may differ and are peculiar to the operations of each company.

In no event shall IPST or its employees and agents have any obligation or liability for damages including, but not limited to, consequential damages arising out of or in connection with any company's use of or inability to use the reported information. IPST provides no warranty or guaranty of results.

Particle Formation of Kraft Smelt in a Fluidized Bed

Jason Huff and Jeff Empie*

Institute of Paper Science and Technology, Atlanta, Georgia

Abstract: Experiments have been conducted to determine the effect of fluidization regime on particle formation mechanism and rate in a fluidized bed molten salt solidifier. Three particle-change mechanisms were considered: attrition, coating, and agglomeration. Fluidization regime was determined to have a significant effect on particle growth rate, but not the mechanism of particle growth. The growth rate of particles in the bed was determined to be the result of both agglomeration and coating, but the effect of agglomeration was determined to be dominant. Fluidization regime had an effect on the size of agglomerates formed, which resulted in differences in particle growth rate. These results were determined to be due to greater mixing and heat transfer of the turbulent bed, which separated particles bound by molten salt and limited the amount of molten-phase salt resident in the system by freezing it more quickly. Attrition of seed particles had no effect on particle formation.

Keywords: Fluidized Bed, Particle Growth, Agglomeration, Coating, Kraft Smelt

Introduction

During the combustion and recovery of spent kraft pulping liquor, the inorganic portion of the liquor forms an extremely hot and caustic molten salt slurry composed mainly of Na_2CO_3 and Na_2S. Because of its corrosiveness, this molten salt slurry, or smelt, is currently allowed to run uncontrolled out of the bottom of the recovery furnace and into a large tank of water (Figure 1) after being broken up with steam jets (Boniface, 1992).

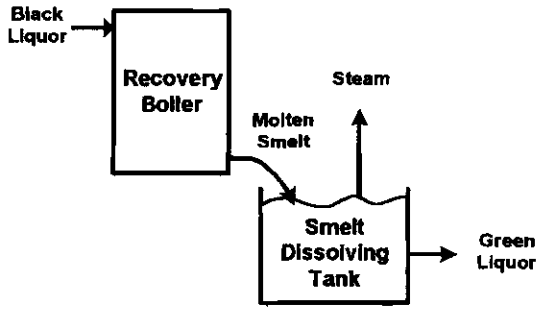

Figure 1. Current Smelt-handling Process

This lack of control over smelt flow leads to a fluctuating concentration of the dissolved smelt or green liquor, which can lead to quality-control problems. Insertion of the molten smelt directly into the aqueous phase of the smelt-dissolving tank also results in the release of sulfur-contaminated steam, which must be scrubbed. This contact of extremely hot molten smelt with water also creates the potential for a smelt-water explosion (Hough, 1991).

- Correspondence should be sent to: 500 10th St., NW, Atlanta, GA 30318

A novel method has been patented by Empie (1996) to solidify the molten smelt, using a fluidized bed, before introducing it to the smelt-dissolving tank where its feed rate can be controlled by conventional means. Previous research by Reeves (1995) has shown that introduction of this solid smelt to the bottom of the smelt-dissolving tank (Figure 2) will cause any steam bubbles that are created to condense and collapse before reaching the surface of the tank, thereby eliminating the need for scrubbing.

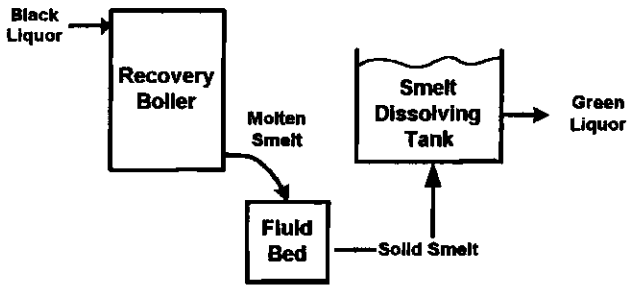

Figure 2. Proposed Smelt-solidification Process

In order for this process to work effectively, particle growth rate in the fluidized bed must be controlled. If random collisions of particles cause shrinkage and the particle size distribution decreases too quickly, then the fluidizing gas will elutriate the bed. Conversely, if the interaction of sticky molten salt in the bed causes particles to grow too fast, then the fluidizing gas will not be able to support the particle size distribution and the bed will defluidize. The rate of change of particle size in the bed will have a large impact on the ability of a fluidized bed solidifier to operate effectively (Kunii and Levenspiel, 1991).

Currently, molten smelt can be found in fluidized bed black liquor combustors where black liquor is sprayed into the fluidized bed and spreads throughout the bed while burning. Though the overall temperature of the bed is maintained below the melting point of smelt to avoid defluidization, there are localized pockets of high temperature created by the combustion of black liquor droplets that result in small pockets of molten smelt. These pockets of molten smelt coat the cooler smelt particles and solidify on them. The population of the bed particles is controlled by removing larger particles that have grown for further processing (Liem and Sheridan, 1982). In a molten smelt solidification process where molten smelt is fed through the freeboard, the molten smelt does not occur in small random and dispersed pockets throughout the bed, but in a continuous localized area in the top of the bed. This can lead to serious process problems if particles grow too quickly (Tardos, Mazzone, and Pfeffer, 1985).

In order to overcome these process-related problems, it is important to understand how bed-operating parameters, such as the type of fluidization, affect particle formation in the bed. Kunii and Levenspiel (1991) describe bubbling beds as having two distinct types of fluidization or fluidizing regimes, bubbling and turbulent. Bubbling fluidization is characterized by large bubbles and large-scale mixing while turbulent fluidization is characterized by smaller bubbles and small-scale mixing. This paper investigates how

these two fluidizing regimes affect particle growth and formation in the presence of changes to a molten salt feed.

Experimental Setup and Procedure

A factorial set of experiments focusing on the effect of fluidization regime on particle growth and formation with changes in the injected molten salt feed temperature and mass flow rate was carried out to evaluate this molten salt solidifier concept. The experimental setup included a fluidized bed solidifier, sampler, and smelt injector (Figure 3).

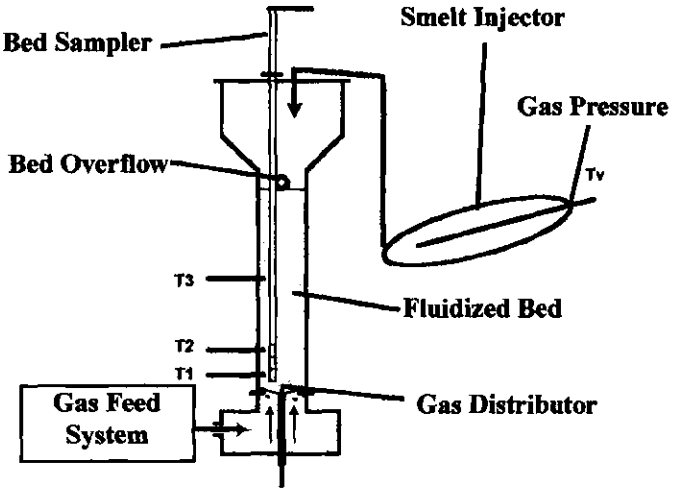

Figure 3. Experimental Setup

The fluidized bed consisted of a cylinder 6.5 cm in diameter and 43.2 cm long in which 2.3 kg of salt of a known particle size distribution was fluidized by air injected through a gas distributor consisting of 24 evenly spaced holes in a metal plate. Into this fluidized bed a stream of molten model smelt was injected, and samples were taken from within the bed at predetermined time intervals. The sampler was designed to remove bed material from the solidifier by allowing it to flow freely into a void space created by twisting the alignment of holes in two concentric cylinders. The opening to this void volume (~1% bed volume) was opened and closed by twisting these concentric cylinders relative to one another. A representative particle size distribution was then determined from this sample to represent the bed. Known particle size distributions were charged to the bed and sampled in order to validate that the samples taken represented the particle size distribution of the bed accurately.

A eutectic combination of $NaNO_3$-KNO3 was used as a model smelt because of the corrosiveness and high temperatures associated with molten kraft smelt (Janz, 1976). Dimensionless groups were generated from system variables that were expected to impact particle growth; these were used to compare the kraft smelt system to the model salt system. These variables can be seen in Equation 1.

$$\frac{d\,d_P}{dt} = f\left(C_{Pg}, C_{Pms}, \mu_g, \mu_{ms}, k_g, k_{ms} d_{Po}, u_0, \rho_g, \rho_{ms}, \rho_P, \Delta T, F_o, \sigma, \Delta H_f, h\right) \quad (1)$$

Using the Buckingham Pi theorem, the resulting dimensionless terms can be seen in Table 1. Representative values for the properties in Equation 1 were used to calculate the values of these dimensionless terms for comparison. These same dimensionless groups were used later to analyze particle growth phenomena in the bed.

A factorial design was used to understand the effect of fluidizing regime on particle growth and formation in the presence of variability in molten salt injection. Samples were taken within each experiment over time to determine particle growth rate and mechanism of formation. Particle growth rate is defined here as the rate of increase in the mean particle diameter, $\bar{d}_P$, where mean particle diameter is taken as the volume weighted mean particle diameter (D_{43}) of the particle size distribution (Sowa, 1992). Mechanism of formation was determined by analyzing the difference between the initial particle size distribution placed into the bed and the resulting distribution after 30 seconds. The conditions used in the factorial design can be seen in Table 2.

Fluidizing gas velocities needed to produce bubbling and turbulent fluidization with a bed mean particle size of 0.63 mm were determined empirically from Kunii and Levenspiel (1991). Levels for molten salt feed rate and temperature were intended to simulate the variability of the molten kraft smelt stream out of the recovery boiler and were chosen according to the safety and operational constraints of the experimental setup used.

Results and Discussion

Particle Growth Rate

The resulting particle growth rates for each of the experimental conditions can be seen in Table 3. An analysis of variance of these results showed a significant decrease in particle growth rate resulting from a change in fluidizing regime (0.18 mm/min).

A linear regression of the dimensionless terms introduced in Table 1 was then calculated using the experimental data. The overall impact of these terms on particle

$$\frac{d\bar{d}_P}{dt} = \frac{\left[\begin{array}{l} 5.6x10^{-5}\,\mathrm{Re}_g - 1.9x10^{-3}Nu + 2.5x10^{-2}\,\mathrm{Pr}_L + 8.4x10^{-4}\,\mathrm{Pr}_g \\ \qquad - 3.9x10^{-7}\left(\dfrac{\mathrm{Re}_L^{\,2}}{We}\right) - 7.7x10^{-14}A + 1.2x10^{-5}B - 0.02026 \end{array}\right]}{\left(\dfrac{\bar{d}_{Po}\rho_L}{\mu_L}\right)} \quad (2)$$

growth rate was then determined by multiplying the coefficients of each dimensionless group, as determined by linear regression, by the average value of that group (Table 1).

The absolute values of these products were then compared to determine the relative importance that each dimensionless group had on particle growth (Table 4). As can be seen in Table 4, the three dimensionless groups with the greatest impact on particle growth rate, Pr (Prandtl), Nu (Nusselt), and Re^2/We (Reynolds^2/Weber), are all indicators of how long the molten salt remains molten in the fluidized bed. The impact of the other four terms was neglected due to their small overall impact.

Prandtl number (Equation 3) was shown to have the greatest impact on particle growth and can be used to describe the ratio of the ability of the molten salt to remain molten relative to its ability to spread over the surface of the particle it is coating.

$$\mathrm{Pr}_L = \frac{C_{P_L}\mu_L}{k_L} = \frac{C_{PL}/k_L}{1/\mu_L} \tag{3}$$

The ability of the molten salt to remain molten is represented by the ratio of the specific heat capacity of the molten salt (C_{Pl}) or the amount of sensible heat energy held in the molten salt divided by the molten salt's thermal conductivity (k_L) or its ability to get rid of this heat energy. The ability of the molten salt to spread over the surface of the particle is represented by the reciprocal molten salt viscosity (μ_L) or the resistance of the molten salt to deformation or spreading. An increase in the spreading of the salt also increases the surface area of the salt and the rate of heat transfer, which decreases the residence time of the salt and thus the time available for the salt to cause agglomeration.

The calculated regression coefficient for Prandtl number is positive, which indicates that an increase in Prandtl number leads to an increase in particle growth rate. This indicates that an increase in the residence time of the molten salt in the bed leads to an increase in particle growth rate. The impact of this number is most likely a decrease in thermal diffusivity and not momentum diffusivity (Incorpera and Dewit, 1990) because the viscosity of the molten salt is a second and third-order term in other groups with much smaller impacts on particle growth (i.e., A and B).

Nusselt number (Equation 4) is an indicator of the rate of heat transfer at the surface of the particle shown mainly by the convection coefficient (h) for heat transfer from the surface of the molten salt.

$$Nu = \frac{h\bar{d}_{Po}}{k_g} \tag{4}$$

The coefficient representing Nusselt number as determined by regression is negative, which indicates that an increase in this number, and thus an increase in heat transfer from the molten salt, leads to a decrease in overall particle growth rate. Once again, the heat transfer rate is a strong determinant of particle growth rate. The rate of heat transfer determines the molten salt's residence time and dispersion of molten salt within the system and thus the opportunities for agglomeration.

Dimensionless group Re^2/We (Equation 5) is a representation of the thickness of molten salt coatings on particle surfaces. An increase in the value of this group leads to a

$$\frac{Re^2}{We} = \frac{\sigma_L \bar{d}_P \rho_g g_c}{\mu_L^2} \tag{5}$$

thinner layer forming on the surface of the particle. This results from a decrease in the viscosity in the denominator and thus a decrease in the ability of the particle to resist deformation, and/or an increase in the surface tension, which increases the tendency of the molten material to spread.

The coefficient for this group is negative which indicates that an increase in this number decreases the overall growth rate of particles. This may be the result of an increase in the rate of heat transfer out of the molten salt and thus its residence time in the bed. By decreasing the thickness of the molten salt coating on bed particles, the molten salt surface area increases, which increases the pathway through which heat is transferred, and the effective heat transfer length over which heat must travel decreases. Both of these acting together increase the heat transfer rate out of the molten salt and thus decrease the residence time of molten salt in the bed.

The results of this regression equation were plotted against actual growth in order to understand how the dimensionless group regression compared. The results of this comparison can be seen in Figure 4. The line extending from the origin represents a slope of one or a 100% correlation between the observed and predicted particle growth rates.

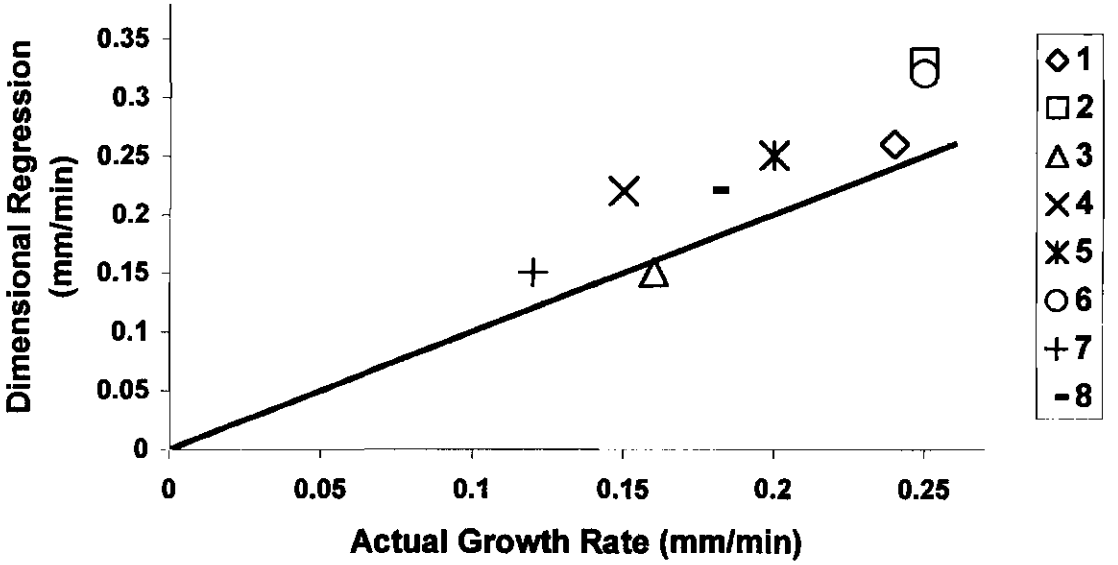

Figure 4. Comparison of Actual and Predicted Particle Growth Rates

As can be seen from Figure 4, there does not appear to be any second-order trend in the data or, in other words, the error existent in the data appears to be the random error resulting from the first and second regressions. Experiments 2, 4, 6, and 8 are all grouped above the line. This could be the result of higher injection velocity of the molten salt stream into the top of the bed that resulted from the doubling of the mass flow rate of molten salt through the same injection tube into the top of the bed. This is a difference between the experimental conditions that would not be accounted for in the regression.

Particle Formation

Changes in the volume of material in individual particle size ranges were determined between the initial particle size distribution and the resulting particle size distribution after particle growth. The mass fraction difference of distributions was analyzed by determining the mean particle diameter of the negative (initial particles-that-grew) and positive (particles-formed) portions of the overall distribution (Figure 5) separately in order to quantify each. This was accomplished by determining the volume moment of the absolute value of the negative distribution to determine the initial mean diameter of the particles-that-grew ($\bar{d}_{P_G}$) and the moment about the positive distribution to determine the mean diameter of the particles-formed ($\bar{d}_{P_F}$).

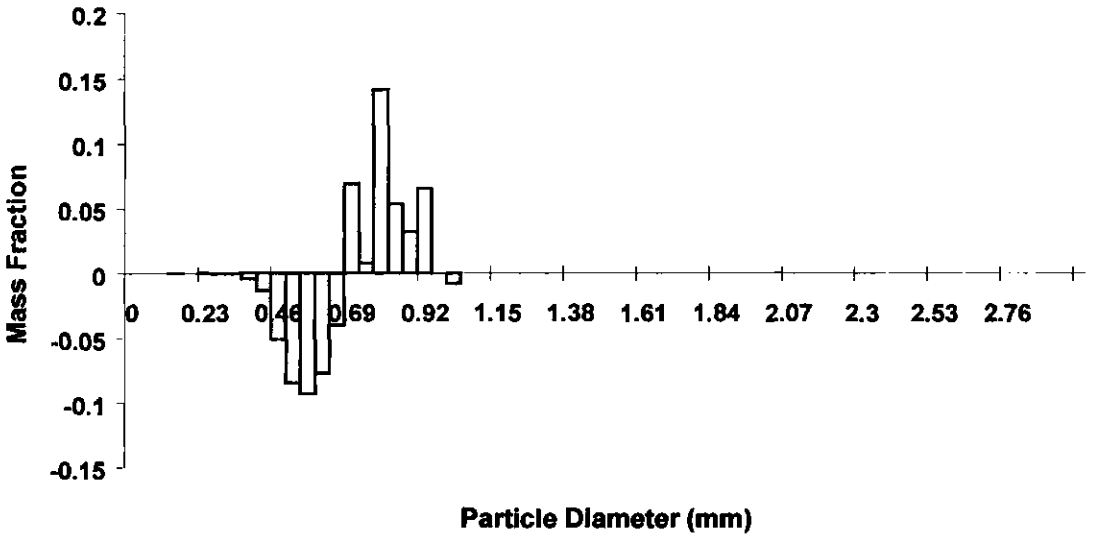

Figure 5. Difference of Distributions

Equation 6 and 7 were used to determine the mean diameters of the particles-that-grew (d_{PG}) and the particles-formed (d_{PF}), respectively.

$$\bar{d}_{P_G} = \sum_{G} |X_i| \left(\frac{d_{P_i} + d_{P_{i+1}}}{2} \right) \qquad (6)$$

$$\bar{d}_{P_F} = \sum_F X_i \left(\frac{d_{P_i} + d_{P_{i+1}}}{2} \right) \tag{7}$$

The results of these calculations can be seen in Table 5. Each is the average of the replicates under that condition. The standard deviation in Table 5 refers to the standard deviation of the average distribution and the standard deviation of the means of those distributions.

The average value of all initial mean diameters from Table 5 is 0.57 mm for both upper and lower samples with a confidence interval 0.03 mm for the upper sample and 0.01 mm for the lower sample. These confidence intervals show that there is no significant difference between the initial mean diameters of the particles-that-grew in either the upper or the lower sample. These values compare well with the number-average initial mean particle diameter of 0.58 mm. This indicates that particle formation in the bed is the result of random particle collisions with the molten feed and with other bed particles.

One notable exception is the initial mean diameter-that-grew of 0.69 mm shown in Experiment 7. This was determined by analysis of the resulting histograms to be the result of a large amount of broken solidified molten salt material forming small particles. These small particles, formed during the breakup of newly solidified material, masked the smaller particles of the initial particle size distribution when the initial particle size distribution was subtracted from the resulting distribution. The elimination of these small particles from the initial particle size distribution resulted in only the large particles of the initial particle size distribution being used to calculate d_{PG}. This resulted in a larger value being calculated for d_{PG}, which is not representative of the true d_{PG}.

There is less consistency among the experiments in the average size of the particles-formed during particle growth. For instance, the average of the mean particle diameters for Experiment 7, which experienced the lowest particle growth rate, is 0.89 mm while for Experiment 6, which experienced the highest growth rate, the average mean diameter is 0.91 mm. This would seem to indicate that particle growth is a function of the rate of agglomeration and not just the size of the agglomerates formed.

The respective volumes of each of these mean-sized particles-formed and particles–that-grew in Table 5 were calculated and compared to determine how many mean particles-that-grew it would take to create a mean-sized particle-formed. This calculation can be seen in Equation 8. The number of times in size that a particle-formed

$$\#\,Particles = \frac{\frac{4}{3}\pi\left(\frac{\bar{d}_{P_F}}{2}\right)^3}{\frac{4}{3}\pi\left(\frac{d_{P_G}}{2}\right)^3} \tag{8}$$

is greater than a particle-that-grew gives an indication of whether or not there is agglomeration and if so, what size agglomerates are formed. The results of these calculations can be seen in Table 6 along with the respective particle growth rate of each experimental condition. As can be seen from Table 6, all of the resulting mean particles-formed are composed of several (2.8 - 4.5) initial particles-that-grew, which shows that agglomeration predominates as a particle growth mechanism in all experiments.

There are two ways that mean particle growth rate can increase by agglomeration: an increase in the rate of agglomerates formed or an increase in the size of agglomerates. The number of particles per agglomerate was plotted against particle growth rate to determine what correlation, if any, existed between the two. This plot can be seen in Figure 6. It shows that there is a weak correlation between the particles per agglomerate or size of agglomerates formed and particle growth rate taken from the sampler. These results indicate that particle growth is the result of both the rate of agglomerate formation and the size of agglomerates formed.

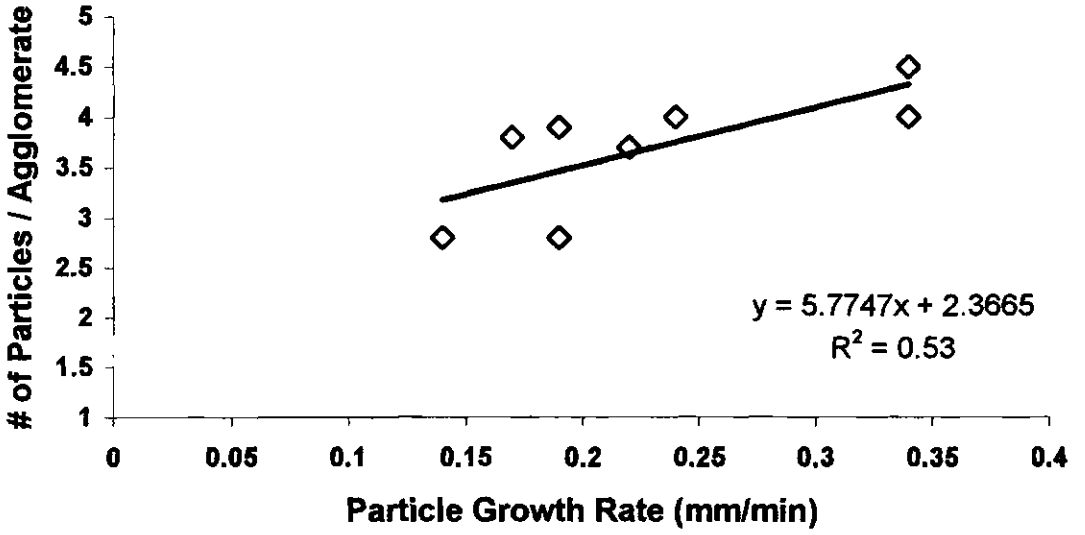

Figure 6. Correlation of Formed Particle Size with Growth Rate

Summary and Conclusions

1. Bed particles grew in the presence of injected molten salt. This growth rate significantly decreased as a result of increased mixing caused by a change from a bubbling to a turbulent fluidizing regime. This particle growth was shown to be mainly the result of heat transfer and solidification rate of the molten salt.

2. Analysis of particle size distributions showed that the largest impact on particle growth resulted from particles combining in the form of agglomerates rather than

being individually coated with molten salt. This was found to be true under all experimental conditions.

3. Particle growth was shown to be the result of both the number and the size of the agglomerates formed.

Nomenclature

d_P	Equivalent spherical diameter
$\bar{d}_P$	Volume weighted mean particle diameter of bed (D_{43})
$\bar{d}_{Po}$	Mean particle diameter of seedbed particles
F_0	Mass feed rate of molten material to the bed
g_c	Dimensional constant used to represent force
h	Heat transfer coefficient
ΔH_f	Latent heat of fusion for salt
J	Dimensional constant used to represent heat
k	Thermal conductivity
T_{mp}	Melting point temperature of the liquid feed
T_{ms}	Temperature of molten salt
ΔT	Difference between T_{ms} and T_{mp}
u_0	Superficial gas velocity
u_1	Bubbling bed superficial gas velocity
u_2	Turbulent bed superficial gas velocity
m_{bed}	Mass of solid material in the fluid bed

Greek

μ	Fluid viscosity
ρ	Density
σ	Surface Tension

Subscripts

L, g	Denotes property of the liquid feed or gas
0, 1, 2	Denotes overall value, into bed, out of bed
ms	Property of the molten stream
s	Surface property of molten particle or solid
G	Denotes particles that grew
F	Denotes particles that formed

References

Boniface, A. "Introduction and Principles of Chemical Recovery," Chemical Recovery in Alkaline Pulping Processes. Third Edition, TAPPI Press, Atlanta, GA (1992).

Empie H. "Kraft Smelt Solidification in a Fluidized Bed Reactor," U.S. Patent 5,545,292 (8/13/96).

Hough, G.W. "Principles of Chemical Recovery," Chemical Recovery in Alkaline Pulping Processes, TAPPI Press, Atlanta, GA (1992).

Incropera, F. and Dewitt, D. Fundamentals of Heat and Mass Transfer, Wiley Publ. (1990).

Janz, G.; Allen; Bansal; Murphy, and Tomkins "Eutectic Data: Safety, Hazards, Corrosion, Melting Points, Composition and Bibliography", Rensselaer Polytechnic Inst. (July 76).

Janz, G. "Thermodynamic and Transport Properties for Molten Salts: Correlation Equations for Critically Evaluated Density, Surface Tension, Electrical Conductance and Viscosity Data," Journal of Chemical and Physical Reference Data Vol. 17 (1988).

Kunii, D.; Levenspiel, O. Fluidization Engineering: Second Edition Butterworth-Heinmann Series in Chemical Engineering (1991).

Liem, A.J ; Sheridan, T.G. "Incremental Kraft Recovery w/ a Fluidized Bed" Pulp & Pap. Can. (Aug 2), 79-84 (1982).

Magnusson; H. Warnqvist, B. "Properties of Sodium Sulfide – Sodium Carbonate Melts", Svensk Papperstidning **17**, 614-616 (1975).

Reeves, R. "Analysis of Gaseous Emissions During Dissolution of Hot, Solidified Smelt in Water" A190 Thesis, Institute of Paper Science and Technology, Atlanta, GA (1995).

Sowa, W.A. "Interpreting Mean Drop Diameters Using Distribution Moments", Atomization & Sprays **2**, 1-15 (1992).

Tardos, G.; Mazzone; Pfeffer. "Destabilization of Fluidized Beds Due to Agglomeration Part II: Experimental Verification", Can. J. Chem. Eng. **63** (June), 384-389 (1985).

Acknowledgment

Portions of this work were used by J.H. as partial fulfillment of the requirements for the Ph.D. degree at the Institute of Paper Science and Technology.

Table 1. Comparison of actual smelt system and model system using the average values of each dimensionless term (Janz, 1988) and (Magnusson and Warnqvist, 1975)

DIMENSIONLESS GROUP	SMELT SYSTEM	MODEL SYSTEM	*Smelt System* / *Model System*
$\frac{\bar{d}_{po} u_0 \rho_g}{\mu_g}$	54	59	0.92
$\frac{h \bar{d}_{po}}{k_g}$	6.3	6.12	1.0
$\frac{C_{PL} \mu_L}{k_L}$ (molten salt)	7.2	16.5	0.44
$\frac{C_{Pg} \mu_g}{k_g}$ (gas)	0.96	0.71	1.4
$\frac{\sigma_l \bar{d}_p \rho_g g_c}{\mu_l^2}$	26200	6500	4.0
$\frac{\Delta T \bar{d}_{Po}^2 \rho_L^2 k_L g_c J}{\mu_L^3}$	3.22×10^9	4.1×10^8	7.9
$\frac{F_0 \Delta H_f \bar{d}_P^2 \rho_L}{\mu_L J}$	76	50	1.52

Table 2. Conditions used in the factorial design of experiments

LEVEL	FLUIDIZING GAS VELOCITY (m/s)	MOLTEN SALT MASS FEED RATE (g/s)	MOLTEN SALT INJECTION TEMPERATURE (°C)
Low	1 (bubbling)	1.1	260
High	2 (turbulent)	2.2	300

Table 3. Mean particle growth rate

CONDITION	U_0 (m/s)	T_i (^{0}C)	F_0 (g/s)	GROWTH RATE (mm/min)
Bubbling Fluidization	1	260	1.1	0.22
	1	260	2.2	0.34
	1	300	1.1	0.24
	1	300	2.2	0.34
Turbulent Fluidization	2	260	1.1	0.17
	2	260	2.2	0.19
	2	300	1.1	0.14
	2	300	2.2	0.19

Table 4. Overall impact of dimensionless terms on particle growth rate ($R^2 = 0.91$)
Classic dimensionless terms Re (Reynolds), Nu (Nusselt), Pr (Prandtl), We (Weber)

DIMENSIONLESS GROUP		MEAN VALUE OF GROUP	COEFFICIENT	PRODUCT	RANK OF IMPORTANCE
Pr_L	$\frac{C_{P_L}\mu_L}{k_L}$	16.5	2.5×10^{-2}	1.8×10^{-1}	1
Nu	$\frac{h\bar{d}_{po}}{k_g}$	6.12	-1.9×10^{-3}	1.2×10^{-2}	2
$\frac{Re_L^2}{We}$	$\frac{\sigma_L \bar{d}_{Po}\rho_g g_c}{\mu_L^2}$	6500	-3.9×10^{-7}	1.0×10^{-2}	3
Re	$\frac{\bar{d}_{po}u_0\rho_g}{\mu_g}$	59	5.6×10^{-5}	3.0×10^{-3}	4
B	$\frac{F_0\Delta H_f \bar{d}_{P_o}^2\rho_L}{\mu_L J}$	50	1.2×10^{-5}	9.3×10^{-4}	5
Pr_g	$\frac{C_{P_g}\mu_g}{k_g}$	0.71	8.4×10^{-4}	8.1×10^{-4}	6
A	$\frac{\Delta T \bar{d}_{Po}^2\rho_L^2 k_L g_c J}{\mu_L^3}$	4.1×10^{8}	-7.7×10^{-14}	2.5×10^{-4}	7

Table 5. Characteristics of particles formed and grown in experiments

EXPERIMENT	PARTICLES THAT GREW		PARTICLES FORMED	
	$\bar{d}_{P_G}$ (mm)	σ (mm)	$\bar{d}_{P_F}$ (mm)	σ (mm)
1	0.55	0.06	0.85	0.1
2	0.54	0.06	0.86	0.08
3	0.55	0.06	0.86	0.04
4	0.57	0.06	0.9	0.11
5	0.55	0.06	0.86	0.09
6	0.55	0.07	0.91	0.09
7	0.69	0.05	0.89	0.08
8	0.59	0.1	0.83	0.06

Table 6. Average number of seed particles per agglomerate at 30 seconds

EXPERIMENT	# Particles / Agglomerate	$\frac{d\bar{d}_P}{dt}$ (mm/min)
1	3.7	0.22
2	4.0	0.34
3	3.8	0.17
4	3.9	0.19
5	4.0	0.24
6	4.5	0.34
7	2.8	0.14
8	2.8	0.19